

# Scaling of Aircraft Incorporating Semi Aeroelastic Hinged Wings

Huaiyuan Gu\*, Fintan Healy, Djamel Rezgui, Mark Lowenberg and Jonathan Cooper  
Department of Aerospace Engineering, University of Bristol  
Queen's Building, University Walk, Bristol, BS8 1TR, UK  
huaiyuan.gu@bristol.ac.uk  
\*Corresponding author

## Abstract

The current demand for highly efficient and 'green' aircraft with less fuel burn calls for innovative wing solutions with improved overall performance. The Semi-Aeroelastic Hinge (SAH) concept has consistently demonstrated promising outcomes in terms of the load alleviation and an improvement in roll performance. This device employs floating folding wingtips as an in-flight load alleviation device such that the hinge will be released during manoeuvres and severe gusts to reduce aerodynamic loads, whilst remain locked for cruise to obtain the optimum wing shape. This paper develops a scaling approach for such wing configurations which allows for the development of scaled wind tunnel models with equivalent aeroelastic behaviour to a full-size aircraft. A set of scaling laws are derived which are employed to scale a reference aircraft incorporating a SAH. Despite significant non-linearities due to large wingtip fold angles, it was found that the linear scaling approach is applicable, and reasonable agreement is obtained between the aeroelastic behaviours of the scaled model and full-size aircraft.

## 1. Introduction

There has been much recent research focusing on improving aircraft performance to reduce fuel burn and environmental impact. The current focus is primarily on increasing wing aspect ratios, leading to a reduction in induced drag. The use of folding wing-tips, as used on the B777-X [1], has been put forwards as a means of solving the problem of airport gate limitations whilst enabling higher aspect ratios. An extension of this concept is to implement floating folding wingtips in-flight which have been shown reduce gust loads and also improving the roll performance of an aircraft [2, 3, 4, 5, 6]. The so-called semi-aeroelastic hinge concept (SAH), whereby the hinge is fixed until a significant amount of turbulence is encountered, as illustrated in Figure 1, is to be employed on the Airbus X-Wing technology demonstrator [7]. Unlike conventional folding wingtips, the hinge is at an angle to the oncoming flow direction, known as the flare angle,  $\Lambda$ , shown in Figure 1. At a positive flare angle,  $\Lambda$ , the local angle of attack on the folding wingtip reduces with the fold angle,  $\theta_f$ . At small fold angles, the change in the local angle of attack can be related to the fold angle,  $\theta_f$ , as [8]

$$\Delta\alpha = -\arctan(\sin\Lambda \tan\theta_f) \quad (1)$$

and for larger fold angles this expression becomes [9]

$$\Delta\alpha = -\sin\Lambda \sin\theta_f \quad (2)$$

When the hinge is released in-flight, the wingtip folds up towards a steady fold angle, known as the coast angle, where the aerodynamic forces and moments are balanced with that due to the wingtip weight. When a new concept is introduced, it is usual to develop prototype test air vehicles to investigate new concepts in wind tunnels or UAVs and, in order to get a full understanding of the behavior, aeroelastic scaling needs to be used to develop an equivalent small aircraft model so that the controlled test characteristics in the wind tunnel can then be used to predict the behaviour for full size models at realistic flight conditions. Such approaches are reasonably standard for conventional aircraft but the occurrence of nonlinearities, such as those that might be found on highly flexible wings undergoing large geometric deflections and those occurring in wings incorporating floating folding wingtips, have received little consideration.

## SCALING OF AIRCRAFT INCORPORATING SEMI AEROELASTIC HINGED WINGS

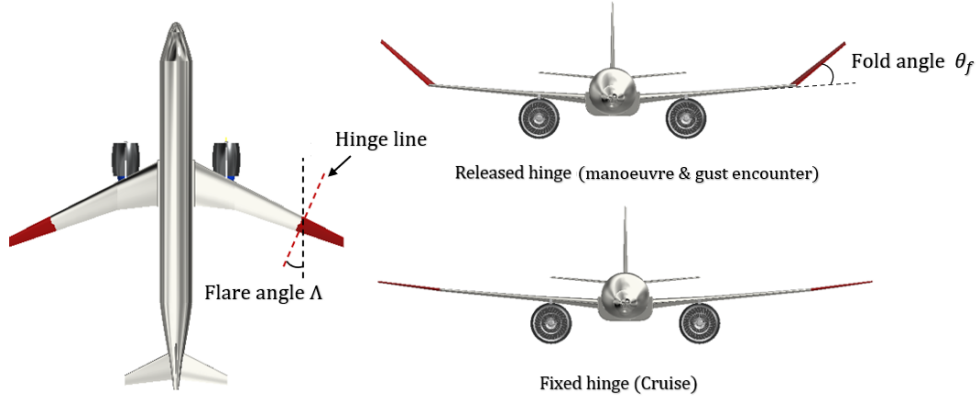


Figure 1: Schematic representation of the semi-aeroelastic hinge (SAH).

A classical scaling approach was employed by Bisplingoff et al. [10], where dimensional analysis was performed on the fundamental aeroelastic equations to derive a set of scaling laws according to the Buckingham  $\pi$  theorem. A very similar approach was implemented by Chester et al. [11] to determine the scaling laws for required for aircraft and corresponding wind-tunnel and free-flight models under compressible and incompressible flows. One common observation is that the similitude requirements for the scaling cannot always be met in practice. For example, the Reynolds number of the scaled-models are often inconsistent to that of the full-size model, which may lead to significant variations in the aerodynamic characteristics i.e. drag, maximum lift coefficient and stall behaviour. Moreover, in the cases where compressibility effects cannot be neglected, such as in transonic and supersonic flight, it is required to match the equivalent Mach number for the scaled model by varying the flight speed, whereas the requirement for the Froude number can no longer be met unless the gravitational constant can be scaled accordingly[12]. A similar conclusion was also reached by Chester et al. [11] that emphasised the limitations of scaling of aircraft operating under compressible flow conditions. Wan et al. [13] developed scaling approaches for highly flexible aircraft that exhibit large deformations by extending the existing scaling laws derived for linear models to address the scaling of geometrically nonlinear structures. An alternative scaling approach for flexible structures was employed by Ricciardi et al. [14] based on the equivalent static loads to match to the nonlinear static response of the full-size model.

This paper presents the development of scaling approaches for high aspect ratio wings incorporating the semi-aeroelastic hinge (SAH) concept. A fundamental aeroelastic analysis is first conducted, followed by a direct dimensional analysis to determine the scaling laws. A set of scaling factors are derived to allow for the aeroelastic behaviour of the scaled model to be consistent to that of the full-size model. The proposed scaling approach is then employed on a reference aircraft model, where the static and dynamic aeroelastic behaviors, including trim angle, wingtip deflection, stability boundaries (flutter), and gust responses, are compared between the scaled model and the full-size model to assess the validity of the approach.

## 2. Scaling methodology

In this section, a set of non-dimensional aeroelastic equations of a flexible wing incorporating semi-aeroelastic hinge are derived using strip theory and Euler-Lagrange's equations of second kind, in which a group of governing quantities are obtained to determine the scaling laws. Considering a swept wing with inner wingspan of  $b_i$ , FWT span of  $b_f$  (as shown in Figure 3), the vertical displacement of the wing can be expressed as [15]

$$Z = \sum_{n=1}^N -\phi_{bi}q_{bi} + \phi_{ti}q_{ti}c(y)e \quad (3)$$

where  $\phi_{bi}$  and  $\phi_{ti}$  represent shape functions of wing bending and torsion.  $q_{bi}$  and  $q_{ti}$  are the generalised coordinates.  $e$  indicates the chordwise distance of an arbitrary point on the wing to the wing elastic axis, which is expressed in terms of the percentage of chord. The kinetic energy can therefore be written in terms of  $\phi_{bi}$ ,  $\phi_{ti}$ ,  $q_{bi}$  and  $q_{ti}$  as

$$T = \frac{1}{2}\rho_m \iint (-\phi_{bi}q_{bi} + \phi_{ti}q_{ti}c(y)e)^2 dA + \frac{1}{2}I_f\dot{\theta}_f^2 \quad (4)$$

## SCALING OF AIRCRAFT INCORPORATING SEMI AEROELASTIC HINGED WINGS

where  $\rho_m$  is the area density of the wing i.e. wing mass/wing area.  $c(y)$  is the chord length at span position of  $y$ .  $I_f$  and  $\dot{\theta}_f$  are the moment of inertia and rate of wingtip fold angle. Therefore, the strain energy possessed by the deformed wing can be defined as

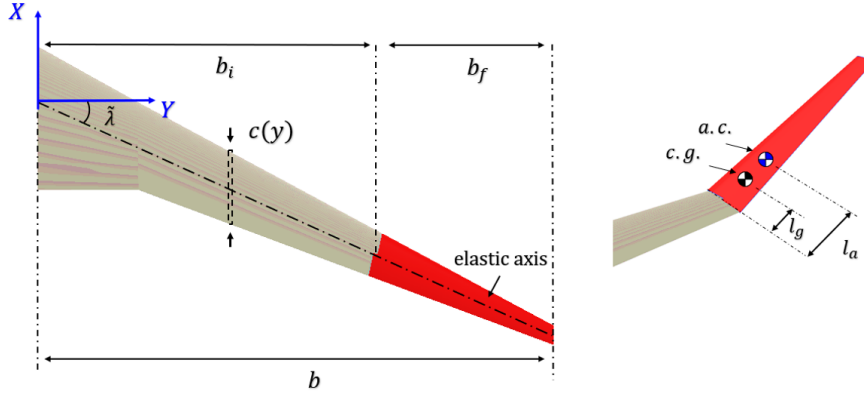


Figure 2: Schematic drawing of the wing model.

$$U = \frac{1}{2} \int_0^{b_i} EI(\phi_{bi}'' q_{bi})^2 dy + \frac{1}{2} \int_0^{b_i} GJ(\phi_{ti}' q_{ti})^2 dy + m_f g l_g \sin \theta_f \quad (5)$$

where (') indicates differentiation with respect to spanwise position  $y$ .  $l_g$  indicates the perpendicular distance from the centre of mass (c.g.) of the wingtip to the hinge axis. The lift forces acting on the inner wing and folding wingtips can be related to the root angle of attack  $\alpha_0$ , fold angle,  $\theta_f$ , wing shapes, and swept angle,  $\tilde{\lambda}$  such that

$$L_{inner} = \frac{1}{2} \rho U^2 \int_0^{b_i} c(y) \left( \alpha_0 + \frac{\phi_{bi} \dot{q}_{bi}}{U} + \underbrace{\phi_{ti} q_{ti} + \phi_{bi}' q_{bi} \sin \tilde{\lambda}}_{\text{twist by bending}} \right) dy \quad (6)$$

$$L_{fwt} = \frac{1}{2} \rho U^2 l_a \int_{b_i}^b c(y) \left( \alpha_0 + \frac{\dot{q}_{bi}}{U} + q_{ti} + \phi_{bi}' q_{bi} \sin \tilde{\lambda} - \sin \Lambda \sin \theta_f \right) dy \quad (7)$$

The classical Lagrangian approach is applied to obtain the equations of motions so that

$$\frac{d}{dt} \frac{\partial L}{\partial \dot{q}_i} + \frac{\partial L}{\partial q_i} = \sum Q_i \quad (8)$$

and then the sum of generalised force,  $\sum Q_i$  due to the lift generated on the inner wing and folding wingtips can be written as

$$\sum Q_i = L_{inner} \frac{\partial r_l}{\partial q_i} + L_{fwt} \frac{\partial r_{fwt}}{\partial q_i} \quad (9)$$

$r_{inner}$  and  $r_{fwt}$  represent the position vectors of the points where the  $L_{inner}$  and  $L_{fwt}$  act on. Substituting Eqs. (3) to (13) into Eq. (8), yields the equations of motions in the form

$$[M] \{\ddot{q}_i\} + [K] \{\dot{q}_i\} = [A_k] \{q_i\} + [A_c] \{\dot{q}_i\} + [A_0] \quad (10)$$

where

## SCALING OF AIRCRAFT INCORPORATING SEMI AEROELASTIC HINGED WINGS

$$q_i = [\cdots, q_{bi}, \cdots, q_{ti}, \cdots, \theta_f]^T \quad (11)$$

The equation of motion for wing bending can be written as

$$\begin{aligned} \rho_m \iint \phi_{bi}^2 dA \ddot{q}_{bi} + EI \int_0^{bi} (\phi_{bi}'')^2 dy q_{bi} &= -\frac{1}{2} \rho U^2 \int_0^b c(y) \phi_{bi} dy \alpha_0 \\ -\frac{1}{2} \rho U \int_0^b c(y) \phi_{bi}^2 dy \dot{q}_{bi} - \frac{1}{2} \rho U^2 \int_0^b c(y) \phi_{bi}' \phi_{bi} \sin \lambda dy q_{bi} &+ Q_{bt} \end{aligned} \quad (12)$$

where  $Q_{bt}$  represents the generalised force coupled with wing bending and torsion. By nondimensionalising the incremental area,  $dA$ , span position,  $y$ , chord length,  $c(y)$ , generalised coordinates,  $q_{bi}$ , using the semi-span,  $b$  yields

$$\begin{aligned} \frac{Mb^3}{S} \iint \phi_{bi}^2 d\bar{A} \ddot{\bar{q}}_{bi} + \frac{EI}{b^2} \int_0^1 (\bar{\phi}_{bi}'')^2 d\bar{y} \bar{q}_{bi} &= -\frac{1}{2} \rho U^2 b^2 \int_0^1 \bar{c}(\bar{y}) \phi_{bi} d\bar{y} \alpha_0 \\ -\frac{1}{2} \rho U b^3 \int_0^1 \bar{c}(\bar{y}) \phi_{bi}^2 d\bar{y} \dot{\bar{q}}_{bi} - \frac{1}{2} \rho U^2 b^3 \int_0^1 \bar{c}(\bar{y}) \bar{\phi}_{bi}' \phi_{bi} \sin \lambda d\bar{y} \bar{q}_{bi} &+ Q_{bt} \end{aligned} \quad (13)$$

$(\bar{\phi}_{bi}')$  and  $(\bar{\phi}_{bi}'')$  indicate the first and second derivatives with respect to the nondimensional length,  $y/b$ . Nondimensionalising the time using the natural frequency of the first mode  $\omega_1$  gives

$$\begin{aligned} \underbrace{\frac{M}{\rho b S}}_{\mu_1} \iint \phi_{bi}^2 d\bar{A} \ddot{\bar{q}}_{bi} + \underbrace{\frac{EI}{\rho b^6 \omega_1^2}}_{\sigma_1} \int_0^1 (\bar{\phi}_{bi}'')^2 d\bar{y} \bar{q}_{bi} &= -\frac{1}{2} \underbrace{\left(\frac{U}{\omega_1 b}\right)^2}_{1/k^2} \int_0^1 \bar{c} \phi_{bi} d\bar{y} \alpha_0 \\ -\frac{1}{2} \underbrace{\frac{U}{\omega_1 b}}_{1/k} \int_0^1 \bar{c} \phi_{bi}^2 d\bar{y} \dot{\bar{q}}_{bi} - \frac{1}{2} \underbrace{\left(\frac{U}{\omega_1 b}\right)^2}_{1/k^2} \int_0^1 \bar{c} \bar{\phi}_{bi}' \phi_{bi} \sin \lambda d\bar{y} \bar{q}_{bi} &+ Q_{bt} \end{aligned} \quad (14)$$

Similarly, the procedure described in Eq. (12) to (14) was undertaken to obtain the non-dimensional equation of motions for the wing torsion and folding wingtip flapping modes, thus

$$\underbrace{\frac{M}{\rho b S}}_{\mu_1} \iint \phi_{ti}^2 x_f^2 d\bar{A} \ddot{\bar{q}}_{ti} + \underbrace{\frac{GJ}{\rho b^6 \omega_1^2}}_{\sigma_1} \int_0^1 (\bar{\phi}_{ti}')^2 d\bar{y} \bar{q}_{ti} = \frac{1}{2} \underbrace{\left(\frac{U}{\omega_1 b}\right)^2}_{1/k^2} \int_0^1 \bar{c} x_a \phi_{ti}^2 d\bar{y} \bar{q}_{ti} + Q_{tb} \quad (15)$$

$$\underbrace{\frac{\omega_1^2 I_f}{m_f g l_g}}_{\mu_3} \ddot{\theta}_f + \cos \theta_f = -\frac{1}{2} \frac{\rho b^3}{m_f} \frac{U^2}{bg} \int_0^1 \sin \Lambda \sin \theta_f \bar{c} l_a d\bar{y} + Q_{fb} \quad (16)$$

where  $Q_{tb}$  and  $Q_{fb}$  indicate the coupled generalised forces. The set of governing quantities that result in Eqs. (14), (15) and (16) need to be matched across the length scales to reach similarity in all dynamic aeroelastic behaviors including: (1) inertia ratio  $\mu$ , (2) nondimensional stiffnesses  $\sigma_1$  and  $\sigma_2$ , (3) reduced frequency  $k$ , (4) Froude number  $Fr$ , and (5) elastic mode shapes  $\phi_{bi}$  and  $\phi_{ti}$ . Note that the aerodynamic similarities such as compressibility and viscous effects are not considered in this derivation. The matching of aerodynamic similarities requires consistent Mach and Reynolds numbers with the full-size model which is difficult to realise in practice. However, it is reasonable to neglect the scaling of compressibility and viscous effects in cases where their influence is relatively small [13, 14]. Note that the damping and stiffness terms of the wingtip flapping motion are associated to the fold angle,  $\theta_f$ , and flare angle,  $\Lambda$ , in a nonlinear manner, as shown in Eq. (16). However, the scaling factors for the angular quantities are equal to unity and therefore, neither fold angle,  $\theta_f$ , nor flare angle,  $\Lambda$ , appear in the scaling laws, suggesting that the linear scaling approach is applicable for folding wingtips, despite the presence nonlinear behaviour in the dynamic responses [16].

### 3. Numerical validation

The scaling methods described in section 2 are applied to scale a reference aircraft model incorporating a semi-aeroelastic hinge, as shown in Figure 3. This model is a business jet type aircraft, which was developed at the University of Bristol to study the effect of large aspect ratios and the SAH concept on flight mechanics behaviour. It will be referred to as the *business high aspect ratio jet investigation* (BHAJI).

Detailed planform geometries and mass configurations are listed in Table 1 and 2. In this study, the scaling factors for mass,  $k_m$ , stiffness,  $k_e$ , velocity,  $k_v$ , and frequency,  $k_\omega$  were chosen as  $\bar{\rho}\lambda^3$ ,  $\bar{\rho}\lambda^5$ ,  $\sqrt{\lambda}$  and  $\frac{1}{\sqrt{\lambda}}$  respectively according to the scaling laws derived in the previous section, where  $\bar{\rho}$  represents the density ratio and the length factor,  $\lambda$ , is taken as 0.2 in this study.



Figure 3: Schematic drawing of the wing model.

Table 1: Planform properties of BHAJI

Planform Parameters	Values		
Span position(m)	0.9	1.8	3.2
LE sweep angle(°)	50	28	28
TE sweep angle(°)	0	0	20.5
Dihedral(°)	0	0	0
Depth to chord ratio	0.15	0.12	0.11
Front spar	0.15	0.15	0.15
Rear spar	0.65	0.65	0.65
Wingspan (m)	18		
Wing area (m <sup>2</sup> )	22.9		
Wing aspect ratio	14		
Fuselage length (m)	14.5		
Fuselage diameter (m)	1.8		
Spanwise hinge position (m)	6.5		

Table 2: Mass configurations

Masses	Values (kg)
Payload	1065
Max. take off mass	10500
Operating empty mass	8100
Max. fuel mass	2600
Engine mass	744
Pylon	300
Horizontal tail	270
Vertical tail	286
Fuselage	2942
Landing gear	400

An aeroelastic model of the BHAJI was created using MSC Nastran[17], with the airframe modelled as a series of beam elements (element code CBEAM in Nastran) with lumped masses attached to replicate the payload, fuel mass and system weights (secondary masses). The aerodynamic forces were computed using the Doublet Lattice Method (DLM) which were transferred to the structure using a beam spline and change accordingly upon the aircraft motions and wing shapes. Static aeroelastic analysis was performed using the inbuilt Nastran routine *SOL144*, to compute the wing deflections of the scaled model under a fixed root angle of attack of 4°. The results were compared to that of the full-size model, as shown in Figure 4, where a reasonable agreement was seen for both hinge conditions. The analysis was repeated for various length scale factors,  $\lambda$ , and it was clear that the scaled model exhibited lower tip displacements and fold angles than that of the full-size model, shown in Figure 5. These differences are mainly attributed to compressibility effects, due to the unmatched Mach number between the scaled models and full-size aircraft, which also led to the inconsistent trim angles as shown in Figure 6.

## SCALING OF AIRCRAFT INCORPORATING SEMI AEROELASTIC HINGED WINGS

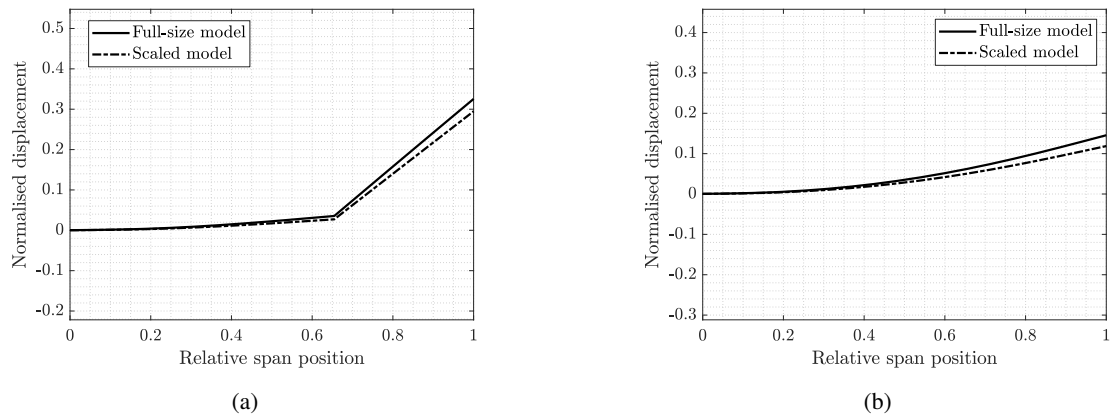


Figure 4: Comparison of (a) wingtip displacement (fixed hinge) and (b) fold angle (free hinge) under  $4^\circ$  root angle of attack under compressible flow.

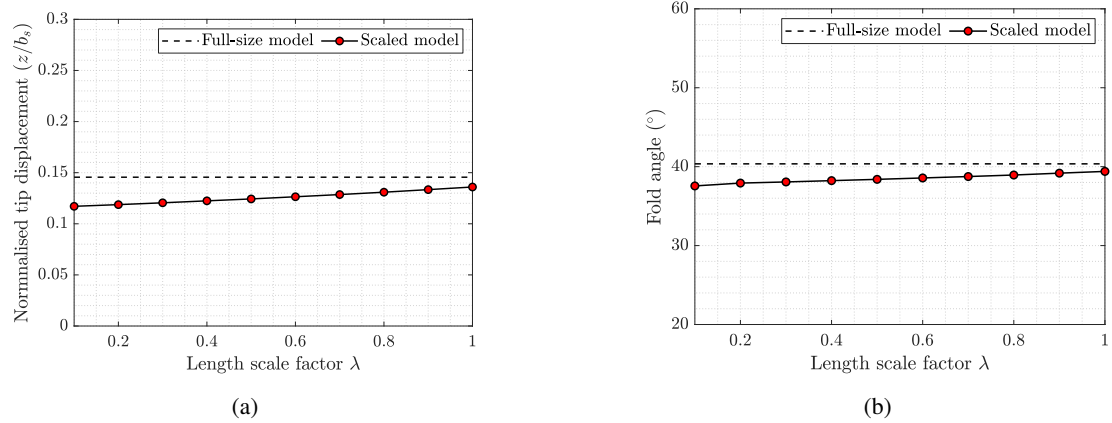


Figure 5: Comparison of (a) wingtip displacement (fixed hinge) and (b) fold angle (free hinge) under  $4^\circ$  root angle of attack under compressible flow.

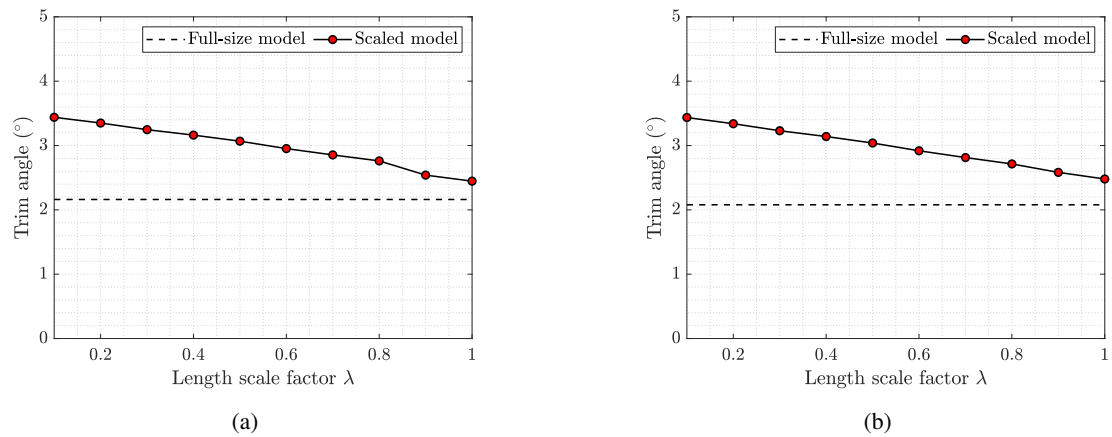


Figure 6: Wing deflection under (a) fixed and (b) free hinge configurations under angle of attack of  $4^\circ$ .

## SCALING OF AIRCRAFT INCORPORATING SEMI AEROELASTIC HINGED WINGS

Flutter analysis was performed using the inbuilt Nastran routine *SOL145* to compute the dynamic stability of both the full-size aircraft and scaled models. For the full-size aircraft, frequencies and damping ratios were computed at speeds between 60 m/s and 230 m/s, as shown in Figure 7 (a) and (b). Whereas for the scaled model, the speed range was adjusted based upon the velocity scaling factor,  $k_v$ , shown in Figure 7 (c) and (d). The obtained frequencies of the scaled model was adjusted by the frequency scaling factor,  $k_\omega$ , and compared to that of the full model shown in Figure 8 (a), where a very good agreement was seen. A reasonably agreement was also found in the damping ratios shown Figure 8 (b), suggesting the scaled models are adequate for predicting dynamic phenomenon such as the flutter speed of the full-size aircraft.

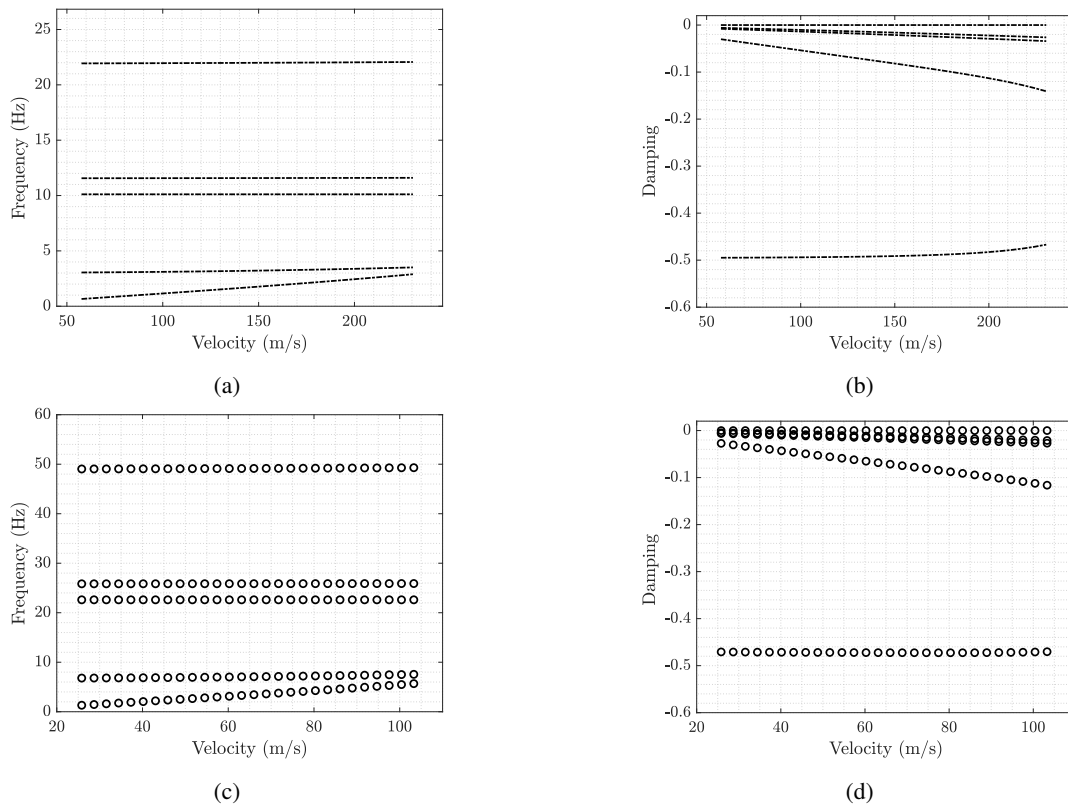


Figure 7: Frequency and damping of (a)(b) the full-size model; (c)(d) the scaled model.

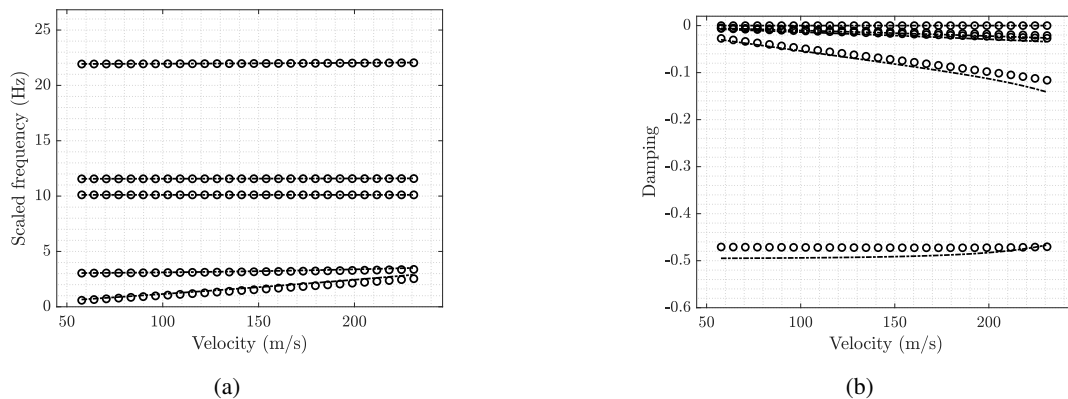


Figure 8: Comparison between the scaled frequency and damping of the scaled model to that of the full-size model. The solid and circular dots represent the results of the full-size and scaled model respectively.

## SCALING OF AIRCRAFT INCORPORATING SEMI AEROELASTIC HINGED WINGS

Analysis was performed using the inbuilt Nastran routine *SOL146* to compare the gust responses of the full-size and scaled model. A discrete gust in the form of one-minus-cosine gust was applied to each model,

$$w_g(t) = \frac{U_{ds}}{2} \left(1 - \cos \frac{2\pi Vt}{L_g}\right) \quad (17)$$

where  $V$  is the true air speed (TAS) and  $U_{ds}$  is the peak gust velocity, which is calculated as

$$U_{ds} = U_{ref} F_g \left(\frac{H}{106.17}\right)^{\frac{1}{6}} \quad (18)$$

$F_g$  is the load alleviation factor which is taken as 1.  $U_{ref}$  is the reference gust velocity which is equal to 17.07 m/s at the sea level and reduces linearly to 13.4 m/s at 4572 m and 7.9 m/s at 15240 m according to Certification Specifications and Acceptable Means of Compliance for Large Aeroplanes (CS - 25) [18]. For the full-size model cruising at 36000ft, the gust length was chosen to be 50 m, where the corresponding gust amplitude was 14 m/s. For the scaled model, the gust length and amplitude were scaled by the length scaling factor,  $\lambda$ , and velocity scaling factor,  $k_v$ , respectively. The time history of the incremental root bending moment is shown in Figure 9 (a), where the results were scaled to achieve consistent units i.e.  $Nm$ . More specifically, the unit was first converted to mass (kg), length(m) and time(s) and scaled accordingly based upon the scaling factors  $k_m$ ,  $\lambda$  and  $k_\omega$  to obtain the scaling factor for the moment. It can be seen that obvious discrepancies were found between the scaled model and full-size model for both root bending moment and wingtip fold angle, see Figure 9 (b). The main cause was due to the inconsistent Mach number between the full-size model and scaled model, which led to different aerodynamic characteristics due to the unmatched compressibility effects.

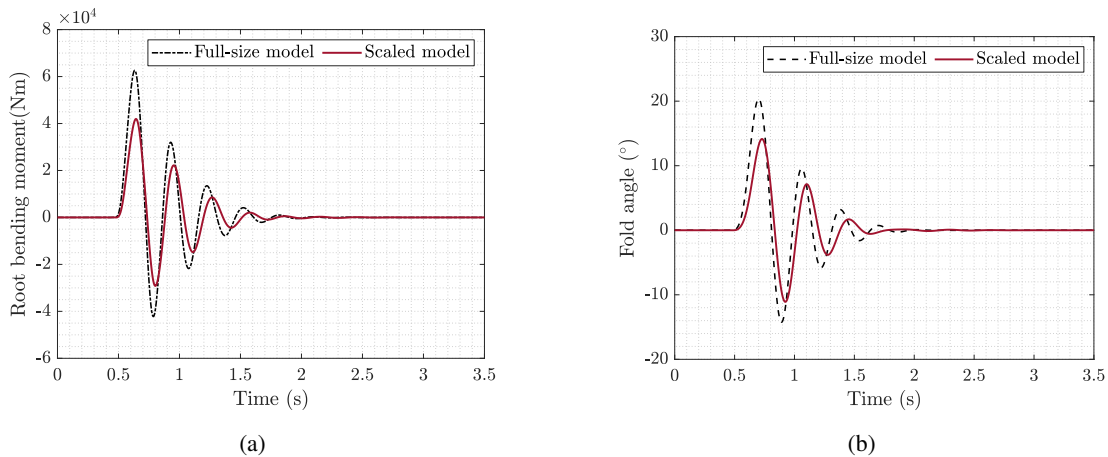


Figure 9: Comparison of gust responses of the full-size and scaled model (a) root bending moment (b) fold angle.

#### 4. Conclusion

Scaling approaches for a wing incorporating a Semi-Aeroelastic Hinge are explored, where a set of scaling laws were derived by performing conventional aeroelastic analysis. It shows that although the wingtip exhibited significant non-linearity in the dynamic behaviours, the linear scaling approaches were found to be applicable for such wing configuration. Furthermore, it is shown that the static behaviour i.e. wing shapes and flutter plots matched well with that of the full-size model. However, it was found to be difficult to provide very accurate matching of the gust responses of the full-size aircraft due to the unscaled compressibility effects.

#### 5. Acknowledgments

The authors acknowledge funding from the DAWS (Development of Advanced Wing Solutions) project (No. 113288) supported by the Innovate UK Aerospace Technology Institute Programme, and funding from the European Union's Horizon 2020 project, Ultra High Aspect Ratio Wing Advanced Research and Designs (U-HARWARD), under grant agreement 886552.

## References

- [1] Mathew Lassen, Chad Douglas, Kelly Thomes Jones, and Terence Boyd Kenning. *Wing Fold Controller*. Office, European Patent, 2018. EP2727829B1.
- [2] Ronald C. M. Cheung, Djamel Rezgui, Jonathan E. Cooper, and Thomas Wilson. Testing of a hinged wingtip device for gust loads alleviation. *Journal of Aircraft*, 55(5):2050–2067, 2018.
- [3] J. E. Cheung. R. C. M., Rezgui. D. Cooper and Wilso. T. Testing of a hinged wingtip device for gust loads alleviation. *Journal of Aircraft*, 55(5):2050â2067, 2018.
- [4] A. Castrichini, J. E. Cooper, T. Wilson, A. Carrella, and Y. Lemmens. Nonlinear negative stiffness wingtip spring device for gust loads alleviation. *Journal of Aircraft*, 54(2):627–641, 2017.
- [5] A. Castrichini, V. Hodigere Siddaramaiah, D. E. Calderon, J. E. Cooper, T. Wilson, and Y. Lemmens. Nonlinear folding wing tips for gust loads alleviation. *Journal of Aircraft*, 53(5):1391–1399, 2016.
- [6] Fintan Healy, Ronald C. Cheung, Theodor Neofet, Mark H. Lowenberg, Djamel Rezgui, Jonathan E. Cooper, Andrea Castrichini, and Tom Wilson. Folding wingtips for improved roll performance. *AIAA Scitech 2021 Forum*, 2021.
- [7] Airbus x-wing future aircraft. [www.compositesworld.com/news/airbus-x-wing-will-test-flapping-wing-tips-multifunctional-trailing-edges-for-future-aircraft](http://www.compositesworld.com/news/airbus-x-wing-will-test-flapping-wing-tips-multifunctional-trailing-edges-for-future-aircraft), 2021. Accessed: 2023-05-24.
- [8] A. Castrichini, V. Hodigere Siddaramaiah, D.E. Calderon, J.E. Cooper, T. Wilson, and Y. Lemmens. Preliminary investigation of use of flexible folding wing tips for static and dynamic load alleviation. *The Aeronautical Journal*, 121(1235):73â94, 2017.
- [9] William Blunt, Fintan Healy, Ronald C. Cheung, Mark H. Lowenberg, and Jonathan E. Cooper. Trailing edge tabs on folding wingtips (fwts) for aircraft roll control. *AIAA SCITECH 2022 Forum*, 2022.
- [10] R.L. Bisplinghoff, H. Ashley, and R.L. Halfman. *Aeroelasticity*. Dover Publications, 1996.
- [11] Jr. and William P. Gilbert Chester H. Wolowicz, James S. Bowman. *Similitude Requirements and Scaling Relationships as Applied to Model Testing*. NASA, 1979.
- [12] Joseph R. Chambers. *Modeling Flight*. NASA, 2020.
- [13] Zhiqiang Wan and Carlos E. S. Cesnik. Geometrically nonlinear aeroelastic scaling for very flexible aircraft. *AIAA Journal*, 52(10):2251–2260, 2014.
- [14] Anthony P. Ricciardi, Charles A. G. Eger, Robert A. Canfield, and Mayuresh J. Patil. Nonlinear aeroelastic-scaled-model optimization using equivalent static loads. *Journal of Aircraft*, 51(6):1842–1851, 2014.
- [15] J.R. Wright and J. E. Cooper. *Introduction to aircraft aeroelasticity and loads*. John Wiley and Sons Ltd, 2<sup>nd</sup> edition, 2014.
- [16] Fintan Healy, Ronald Cheung, Djamel Rezgui, Jonathan Cooper, Thomas Wilson, and Andrea Castrichini. On the effect of geometric nonlinearity on the dynamics of flared folding wingtips. *Journal of Aircraft*, 2023.
- [17] MSC Software GmbH. Msc nastran version: 2019, 2019.
- [18] Cs-25 certification specifications for large aeroplanes. *European Aviation Safety Agency (EASA)*, 2003.